# The linkup of mono-elemental solutions to the SI using INAA: a measurement procedure and the achievable uncertainty

# Title page

Names of the authors: Giancarlo D'Agostino[(1)], Luigi Bergamaschi[(1)], Marco Di Luzio[(1,2)], Janine Noordmann[(3)], Massimo Oddone[(2)] and Olaf Rienitz[(3)]

Title: The linkup of mono-elemental solutions to the SI using INAA: a measurement procedure and the achievable uncertainty

Affiliation(s) and address(es) of the author(s): (1) Istituto Nazionale di Ricerca Metrologica (INRIM) - Unit of Radiochemistry and Spectroscopy, c/o Department of Chemistry, University of Pavia, via Taramelli 12, 27100 Pavia, Italy; (2) Department of Chemistry – Radiochemistry Area, University of Pavia, via Taramelli 12, 27100 Pavia, Italy; (3) Physikalisch-Technische Bundesanstalt (PTB), Bundesallee 100, 38116 Braunschweig, Germany

E-mail address of the corresponding author: g.dagostino@inrim.it

# The linkup of mono-elemental solutions to the SI using INAA: a measurement procedure and the achievable uncertainty

D'Agostino G.[1], Bergamaschi L.[1], Di Luzio M.[1,2], Noordmann J.[3], Oddone M.[2] and Rienitz O.[3]

[1]*Istituto Nazionale di Ricerca Metrologica (INRIM), via Taramelli 12, 27100 Pavia, Italy*

[2]*Department of Chemistry, University of Pavia, via Taramelli 12, 27100 Pavia, Italy*

[3]*Physikalisch-Technische Bundesanstalt (PTB), Bundesallee 100, 38116 Braunschweig, Germany*

## Abstract

The possibility of using neutron activation analysis to link up a secondary to a primary mono-elemental solution was investigated. A procedure was developed for the determination of the ratio between the mass fractions of two solutions. The use of a monitor element was essential to limit the effect of the non-uniformity of the neutron flux during irradiation. The proposed procedure was tested in the case of two molybdenum solutions having the same mass fraction. Although the experiment did not reach the goal, possible ways are suggested to reach the target expanded uncertainty of 0.1 %.

## Keywords

Neutron activation analysis; metrological traceability; reference solution; molybdenum.

## Introduction

Mono-elemental solutions with a mass fraction of 1 g $kg^{-1}$ are being used in almost every chemical laboratory in social, medical and industrial fields to calibrate analytical measurements. The accuracy of those solutions is essential for the reliability and comparability of the applied analyses.

Due to the importance of these calibration solutions, traceability to the SI is necessary. Several national metrology institutes (NMIs) or designated institutes (DIs) provide traceability by the use of high purity solid materials ($w_{pur} \geq 0.999$ g $g^{-1}$) with completely known impurities (metals and non-metals), yielding a purity with an associated expanded uncertainty of less than 0.01 %. In some cases, the distribution of selected impurities among subsamples of the solid materials have been also investigated [1]. Based on these solid materials, primary reference solutions with an expanded uncertainty associated with the mass fraction of less than 0.05 % are gravimetrically prepared and metrologically monitored by NMIs [2].

As the pure and fully characterized materials and the primary solutions have a limited availability and are very valuable concerning the characterization and preparation process, secondary solutions are prepared using pure materials usually only characterized regarding metallic impurities. Therefore, these secondary solutions must be linked up to the primary solutions. The expanded measurement uncertainty of the linkup must be less than 0.1 % to achieve a calibration measurement of commercial solutions with an expanded uncertainty associated with the mass fraction of 0.3 %. Overall, this procedure demonstrates an unbroken chain of calibrations to link up the measurement results in the field to the SI [3].

In this framework, high precision measurements are needed to link up the solutions with a relative expanded uncertainty of less than 0.1 %. In most cases, those measurements are being performed using the inductively coupled plasma optical emission spectrometry (ICP OES) technique.

Given that the application of instrumental neutron activation analysis (INAA) technique is missing in this field, a measurement procedure is suggested and the related measurement model is obtained from the neutron activation equation. In addition, the

proposed procedure was experimentally tested in the case of two Mo solutions having the same mass fraction, i.e. when the ratio is expected to be the unit value.

## Measurement procedure and model

The aim of the measurement is to link up an elemental solution ES1 to an elemental solution ES2 having mass fractions $w_{ES1}(E)$ and $w_{ES2}(E)$ of an element E by determining the ratio

$$\tau = \frac{w_{ES1}(E)}{w_{ES2}(E)} \quad (1)$$

with a relative expanded uncertainty of 0.1 %.

To accomplish this aim, two measurement solutions, mS1 and mS2, are stocked in two different containers by adding a sample (aliquot) of a monitor solution MS having a mass fraction $w_{MS}(E_M)$ of a monitor element $E_M$ to a sample of each elemental solution. Two sub-samples of the measurement solutions, mS1,s and mS2,s, are used in the neutron activation experiment.

To achieve the target uncertainty, attention has to be given to the evaporation of the solution during handling. The elemental solution starts to evaporate with a mass rate $\alpha_{ES}$ when it is transferred from its bottle to the container. After a time $t_{MS}$, the monitor solution is pipetted into the container to obtain the final measurement solution. The solution carries on evaporating during a time $t_{mS}$, with a mass rate $\alpha_{mS}$, until a sub-sample is taken and pipetted into an irradiation vial.

Hence, when the sub-samples are taken, the masses of the measurement solutions are $m_{mS1} = m_{ES1} - \alpha_{E1}\, t_{MS1} + m_{1,MS} - \alpha_{mS1}\, t_{mS1}$ and $m_{mS2} = m_{ES2} - \alpha_{E2}\, t_{MS2} + m_{2,MS} - \alpha_{mS2}\, t_{mS2}$, where $m_{ES1}$, $m_{ES2}$ are the masses of the samples of ES1, ES2 and $m_{1,MS}$, $m_{2,MS}$ are the additional masses of MS.

The mass fractions of E and $E_M$ in the measurement solutions are

$$w_{\mathrm{mS1}}(\mathrm{E}) = \frac{w_{\mathrm{ES1}}(\mathrm{E})}{1+\dfrac{m_{1,\mathrm{MS}}-m_{\mathrm{ev1}}}{m_{\mathrm{ES1}}}},\ w_{\mathrm{mS2}}(\mathrm{E}) = \frac{w_{\mathrm{ES2}}(\mathrm{E})}{1+\dfrac{m_{2,\mathrm{MS}}-m_{\mathrm{ev2}}}{m_{\mathrm{ES2}}}} \tag{2}$$

and

$$w_{\mathrm{mS1}}(\mathrm{E_M}) = \frac{w_{\mathrm{MS}}(\mathrm{E_M})}{1+\dfrac{m_{\mathrm{ES1}}-m_{\mathrm{ev1}}}{m_{1,\mathrm{MS}}}},\ w_{\mathrm{mS2}}(\mathrm{E_M}) = \frac{w_{\mathrm{MS}}(\mathrm{E_M})}{1+\dfrac{m_{\mathrm{ES2}}-m_{\mathrm{ev2}}}{m_{2,\mathrm{MS}}}}, \tag{3}$$

respectively, where $m_{\mathrm{ev1}} = \alpha_{\mathrm{E1}}\, t_{\mathrm{MS1}} + \alpha_{\mathrm{mS1}}\, t_{\mathrm{mS1}}$ and $m_{\mathrm{ev2}} = \alpha_{\mathrm{E2}}\, t_{\mathrm{MS2}} + \alpha_{\mathrm{mS2}}\, t_{\mathrm{mS2}}$ are the evaporated masses.

The number of atoms of an isotope $^{i}\mathrm{E}$ of E and of an isotope $^{i}\mathrm{E_M}$ of $\mathrm{E_M}$ in mS1,s and mS2,s are

$$n_{\mathrm{mS1,s}}(^{i}\mathrm{E}) = \frac{x(^{i}\mathrm{E})\, N_{\mathrm{A}}\, w_{\mathrm{mS1}}(\mathrm{E})\, m_{\mathrm{mS1,s}}}{M(\mathrm{E})},\ n_{\mathrm{mS2,s}}(^{i}\mathrm{E}) = \frac{x(^{i}\mathrm{E})\, N_{\mathrm{A}}\, w_{\mathrm{mS2}}(\mathrm{E})\, m_{\mathrm{mS2,s}}}{M(\mathrm{E})}, \tag{4}$$

and

$$n_{\mathrm{mS1,s}}(^{i}\mathrm{E_M}) = \frac{x(^{i}\mathrm{E_M})\, N_{\mathrm{A}}\, w_{\mathrm{mS1}}(\mathrm{E_M})\, m_{\mathrm{mS1,s}}}{M(\mathrm{E_M})},\ n_{\mathrm{mS2,s}}(^{i}\mathrm{E_M}) = \frac{x(^{i}\mathrm{E_M})\, N_{\mathrm{A}}\, w_{\mathrm{mS2}}(\mathrm{E_M})\, m_{\mathrm{mS2,s}}}{M(\mathrm{E_M})}, \tag{5}$$

respectively, where $m_{\mathrm{mS1,s}}$ and $m_{\mathrm{mS2,s}}$ are the masses of mS1,s and mS2,s, $N_{\mathrm{A}}$ is the Avogadro constant, $x(^{i}\mathrm{E})$ and $x(^{i}\mathrm{E_M})$ are the mole fractions of $^{i}\mathrm{E}$ and $^{i}\mathrm{E_M}$, $M(\mathrm{E})$ and $M(\mathrm{E_M})$ are the molar masses of E and $\mathrm{E_M}$, respectively. Here and hereafter the subscript M refers to the monitor element.

From (1), (2) and (4) it follows

$$\tau = \frac{\left(1+\dfrac{m_{1,\mathrm{MS}}-m_{\mathrm{ev1}}}{m_{\mathrm{ES1}}}\right)\dfrac{n_{\mathrm{mS1,s}}(^{i}\mathrm{E})}{m_{\mathrm{mS1,s}}}}{\left(1+\dfrac{m_{2,\mathrm{MS}}-m_{\mathrm{ev2}}}{m_{\mathrm{ES2}}}\right)\dfrac{n_{\mathrm{mS2,s}}(^{i}\mathrm{E})}{m_{\mathrm{mS2,s}}}}. \tag{6}$$

The two sub-samples of the measurement solutions, mS1,s and mS2,s, are co-irradiated in a neutron flux to activate the target isotopes $^{i}$E and $^{i}$E$_{M}$.

The counting of the $\gamma$-photons emitted during the radioactive decay of the radionuclide produced by activation of the target isotope $^{i}$E allows to quantify the ratio

$$\frac{n_{\mathrm{mS1,s}}(^{i}\mathrm{E})}{n_{\mathrm{mS2,s}}(^{i}\mathrm{E})} = \kappa_{\mathrm{td}}\ \kappa_{\mathrm{R}}\ \kappa_{\varepsilon}\ \kappa_{\mathrm{ss}}\ \kappa_{\mathrm{sa}}\ \kappa_{\mathrm{g}}\ \frac{C_{\mathrm{mS1,s}}(t_{\mathrm{d\,mS1,s}})}{C_{\mathrm{mS2,s}}(t_{\mathrm{d\,mS2,s}})}\ , \qquad (7)$$

where $C(t_{\mathrm{d}})$ is the full-energy $\gamma$-peak detection count rate at a time $t_{\mathrm{d}}$ after the end of the irradiation; here and hereafter, the subscripts mS1,s and mS2,s are occasionally omitted in $C(t_{\mathrm{d}})$. The correction factors $\kappa_{\mathrm{td}} = e^{-\lambda(t_{\mathrm{d\,mS2,s}} - t_{\mathrm{d\,mS1,s}})}$, $\kappa_{\mathrm{R}} = R_{\mathrm{mS2,s}} / R_{\mathrm{mS1,s}}$, $\kappa_{\varepsilon} = \varepsilon_{\mathrm{mS2,s}} / \varepsilon_{\mathrm{mS1,s}}$, $\kappa_{\mathrm{ss}} = k_{\mathrm{ss\,mS2,s}} / k_{\mathrm{ss\,mS1,s}}$, $\kappa_{\mathrm{sa}} = k_{\mathrm{sa\,mS2,s}} / k_{\mathrm{sa\,mS1,s}}$ and $\kappa_{\mathrm{g}} = k_{\mathrm{g\,mS2,s}} / k_{\mathrm{g\,mS1,s}}$ take the differences of decay time, reaction rate, detection efficiency, self-shielding, self-absorption and geometry of the sub-samples into account.

In detail, $\lambda$ is the decay constant of the produced radionuclide, $R$ is the reaction rate per target isotope $^{i}$E, $\varepsilon$ is the detection full-energy $\gamma$ efficiency for a point-like source located at the center of mass of the sub-sample, $k_{\mathrm{ss}}$, $k_{\mathrm{sa}}$, and $k_{\mathrm{g}}$ are the neutron self-shielding, the gamma self-absorption and the geometry factors, respectively.

It is worth to note that in the case of a radionuclide which emits $\gamma$-photons with several energies E$_{\gamma}$, best results are achieved by using in (7) the mean value of the count rate ratios, $\left.\frac{C_{\mathrm{mS1,s}}(t_{\mathrm{d\,mS1,s}})}{C_{\mathrm{mS2,s}}(t_{\mathrm{d\,mS2,s}})}\right|_{\mathrm{m}}$, obtained with different E$_{\gamma}$.

The $\gamma$-counting is carried out using germanium detectors. The count rate $C(t_{\mathrm{d}})$ is obtained by averaging $n$ values, $C_i(t_{\mathrm{d}})$, acquired in a $\gamma$-spectrometry sequence starting at a decay time $t_{\mathrm{d\,1}}$ after the end of the irradiation and consisting of $n$ consecutive counts performed during the decay of the produced radionuclide. More explicitly, each $i^{\mathrm{th}}$ count rate value, $C_i(t_{\mathrm{d}})$, extrapolated to $t_{\mathrm{d}}$ from the $i^{\mathrm{th}}$ count of the sequence, starting at $t_{\mathrm{d}\,i}$ and lasting $t_{\mathrm{c}\,i}$, is

$$C_i(t_d) = \frac{\lambda\, n_{c\,i}}{e^{-\lambda\,(t_{d\,i}-t_d)}\,(1-e^{-\lambda\,t_{c\,i}})}\,\frac{t_{c\,i}}{t_{c\,i}-t_{dead\,i}}, \qquad (8)$$

where $n_{c\,i}$ and $t_{dead\,i}$ are the net count of the full-energy $\gamma$-peak and the detection dead time of the $i^{th}$ count, respectively.

In the case of a $1/E^{1+\alpha}$ epithermal spectrum and if the target isotope $^{i}$E is activated via a (n,$\gamma$) reaction having a cross section with a $E^{-1/2}$ energy dependence, the reaction rate can be described using the Høgdahl convention [4], $R = \Phi_{ep}\,\sigma_{0,E}\,(f + Q_{0,E}(\alpha))$, where $\Phi_{ep}$ is the epithermal neutron flux, $f = \Phi_{th}/\Phi_{ep}$ is the thermal (sub-cadmium) to epithermal neutron flux ratio, $\sigma_{0,E}$ is the (n,$\gamma$) cross section of $^{i}$E at 0.0253 eV and

$$Q_{0,E}(\alpha) = (Q_{0,E} - 0.429)\overline{E}_r^{-\alpha} + \frac{0.429}{(2\alpha+1)\,0.55^{\alpha}}. \qquad (9)$$

In (9) $Q_{0,E}$ is the ratio between the resonance integral of $^{i}$E for a $1/E$ epithermal spectrum, $I_{0,E}$, and$\sigma_{0,E}$, and $\overline{E}_r$ is the effective resonance energy of $^{i}$E [5].

Thus, the characteristics of the neutron energy spectrum affect the $\kappa_R$ correction factor according to

$$\kappa_R = \frac{\Phi_{ep2}(f_2 + Q_{0,E}(\alpha_2))}{\Phi_{ep1}(f_1 + Q_{0,E}(\alpha_1))}, \qquad (10)$$

where $\Phi_{ep1}$, $f_1$, $\alpha_1$ and $\Phi_{ep2}$, $f_2$, $\alpha_2$ are referred to the irradiation positions of mS1,s and mS2,s, respectively.

Several methods have been developed and used to measure the neutron flux parameters; as examples, (i) the “Cd-covered multi-monitor”, the “Cd-ratio for multi-monitor” and the “bare multi-monitor” methods for $\alpha$, (ii) the “Cd-ratio” for $\Phi_{ep}$ and $f$, (iii) the “bare bi-isotopic monitor” method for $f$ [5]. These methods are usually applied offline, i.e. before (or after) the experiment, by assuming that the neutron energy spectrum remains constant and do not depend on the irradiation samples.

In our case, since the $\kappa_R$ value is required with a relative expanded uncertainty of less than 0.1 %, online information is valuable. To reach this aim, the monitor solution is added to the elemental solution. If the Høgdahl convention applies to the target isotope $^{i}E_M$,

$$\kappa_{M\text{-}R} = \frac{\Phi_{ep2}(f_2 + Q_{0,EM}(\alpha))}{\Phi_{ep1}(f_1 + Q_{0,EM}(\alpha))}. \quad (11)$$

From (10) and (11) it follows

$$\kappa_R = \kappa_{M\text{-}R} \frac{1 + \dfrac{\alpha_Q\, Q_{0,E}(\alpha)}{f_1 + Q_{0,E}(\alpha)}}{1 + \dfrac{\alpha_Q\, Q_{0,E}(\alpha)}{f_1(1+\alpha_f) + Q_{0,E}(\alpha)}}, \quad (12)$$

where $\alpha_Q = \dfrac{Q_{0,EM}(\alpha) - Q_{0,E}(\alpha)}{Q_{0,E}(\alpha)}$ and $\alpha_f = \dfrac{f_2 - f_1}{f_1}$.

The counting of the $\gamma$-photons emitted during the radioactive decay of the radionuclide produced by activation of the target isotope $^{i}E_M$ allows to determine

$$\kappa_{M\text{-}R} = (\kappa_{M\text{-}td}\ \kappa_{M\text{-}\varepsilon}\ \kappa_{M\text{-}ss}\ \kappa_{M\text{-}sa}\ \kappa_{M\text{-}g})^{-1} \frac{C_{M\text{-}mS2,s}(t_{d\,M\text{-}mS2,s})}{C_{M\text{-}mS1,s}(t_{d\,M\text{-}mS1,s})} \frac{n_{mS1,s}(^{i}E_M)}{n_{mS2,s}(^{i}E_M)}. \quad (13)$$

According to (3) and (5), the ratio

$$\frac{n_{mS1,s}(^{i}E_M)}{n_{mS2,s}(^{i}E_M)} = \frac{m_{mS1,s}\left(1 + \dfrac{m_{ES2} - m_{ev2}}{m_{2,MS}}\right)}{m_{mS2,s}\left(1 + \dfrac{m_{ES1} - m_{ev1}}{m_{1,MS}}\right)}. \quad (14)$$

In conclusion, the measurement model adopted to link up ES1 to ES2 is obtained from (6), (7), (12), (13) and (14):

$$\tau = \frac{m_{\mathrm{ES2}}}{m_{\mathrm{ES1}}}\frac{m_{1,\mathrm{MS}}}{m_{2,\mathrm{MS}}}\frac{C_{\mathrm{mS1,s}}(t_{\mathrm{d\,mS1,s}})}{C_{\mathrm{mS2,s}}(t_{\mathrm{d\,mS2,s}})}\frac{C_{\mathrm{M\text{-}mS2,s}}(t_{\mathrm{d\,M\text{-}mS2,s}})}{C_{\mathrm{M\text{-}mS1,s}}(t_{\mathrm{d\,M\text{-}mS1,s}})} \times \beta_{\mathrm{R}}\,\kappa_{\mathrm{td}}\,\kappa^{-1}_{\mathrm{M\text{-}td}}\,\kappa_{\mathrm{ss}}\kappa^{-1}_{\mathrm{M\text{-}ss}}\,\kappa_{\mathrm{sa}}\kappa^{-1}_{\mathrm{M\text{-}sa}}\,\kappa_{\mathrm{g}}\kappa^{-1}_{\mathrm{M\text{-}g}}\,\kappa_{\varepsilon}\kappa^{-1}_{\mathrm{M\text{-}\varepsilon}}\,, \quad (15)$$

where $\beta_{\mathrm{R}} = \dfrac{1+\dfrac{\alpha_{\mathrm{Q}}\,Q_{0,\mathrm{E}}(\alpha)}{f_1+Q_{0,\mathrm{E}}(\alpha)}}{1+\dfrac{\alpha_{\mathrm{Q}}\,Q_{0,\mathrm{E}}(\alpha)}{f_1(1+\alpha_{\mathrm{f}})+Q_{0,\mathrm{E}}(\alpha)}}$.

It is remarkable that the result is independent on the masses of the evaporated solutions $m_{\mathrm{ev1}}$, $m_{\mathrm{ev2}}$, on the masses of the irradiated sub-samples $m_{\mathrm{mS1,s}}$, $m_{\mathrm{mS2,s}}$ and on the epithermal flux at the irradiation positions $\Phi_{\mathrm{ep1}}$, $\Phi_{\mathrm{ep2}}$. Moreover, in case of (i) large $f$, (ii) $Q_{0,\mathrm{EM}}(\alpha) \cong Q_{0,\mathrm{E}}(\alpha)$ or (iii) $f_1 \cong f_2$, the result becomes less affected by the $f$, $\alpha$, $\overline{E}_{\mathrm{r}}$, $Q_{0,\mathrm{E}}$, and $Q_{0,\mathrm{EM}}$ values.

## Experimental

The proposed procedure was tested using a Mo solution having a mass fraction $w(\mathrm{Mo}) \approx 1$ g kg$^{-1}$. In this preliminary experiment, a Co solution having a mass fraction $w(\mathrm{Co}) \approx 1$ g kg$^{-1}$ was adopted as the monitor solution. The Mo and Co solutions were obtained using ultrapure ammonium molybdate tetrahydrate, $(NH_4)_6Mo_7O_{24} \cdot 4\,H_2O$, in water and ultrapure Co metal in 0.5 mol L$^{-1}$ nitric acid, respectively.

A single measurement solution, mS, was prepared in a container by adding the Co solution to the Mo solution. Two sub-samples were taken and used for the neutron irradiation. This mimics the application of the procedure in the case of two Mo solutions having the same mass fraction, i.e. $w_{\mathrm{ES1}}(\mathrm{E}) = w_{\mathrm{ES2}}(\mathrm{E})$, $m_{\mathrm{ES1}} = m_{\mathrm{ES2}}$, $m_{1,\mathrm{MS}} = m_{2,\mathrm{MS}}$. To attain the objective, (15) must be satisfied, i.e. $\tau = 1$, with a relative expanded uncertainty of 0.1 %.

The $\tau$ value was determined by counting (i) the 140.51 keV $\gamma$-photons emitted during the radioactive decay of $^{99}$Mo and $^{99\mathrm{m}}$Tc in equilibrium conditions and produced by

activation of $^{98}$Mo via the (n,γ) neutron capture reaction, and (ii) the 1173.23 keV and 1332.49 keV γ-photons emitted during the radioactive decay of $^{60}$Co produced by activation of $^{59}$Co via the (n,γ) neutron capture reaction.

### *Preparation of the measurement solution*

The measurement solution was prepared by pipetting the Co solution to a 25 mL polytetrafluoroethylene (PTFE) flask filled with the Mo solution. To correct for the effect of the evaporation, the mass of the measurement solution, $m_{mS}$, was recorded continuously during its preparation with a sampling frequency of 1 Hz. The data were collected using a digital analytical balance having a resolution of 0.01 mg and calibrated with SI-traceable weights. It is noteworthy that, although the buoyancy affects the weighing of the solution, the ratios of the masses in the model (15) eliminates the effect on $\tau$. Therefore, the weighed masses were not corrected for buoyancy.

The room temperature during the preparation was 26 °C. After setting to zero (tare) the reading of the balance with the empty flask, (i) 21 mL of Mo solution, (ii) 125 μL of Co solution and (iii) 6 mL of Mo solution were consecutively added at 179 s, 532 s and 993 s, respectively. The balance drift during the recording session was −0.02 mg.

A straight line was fitted to the data collected between (i) 223 s and 524 s, (ii) 623 s and 919 s, (iii) 1025 s and 1285 s. The evaporation rates were found to be $2.1 \times 10^{-6}$ g s$^{-1}$, $2.0 \times 10^{-6}$ g s$^{-1}$ and $3.3 \times 10^{-6}$ g s$^{-1}$. According to the fitted data, the masses of the added solutions at steps (i), (ii) and (iii) were $m_{ES}$ = 20.96218(4) g, $m_{MS}$ = 0.12572(4) g and $m_{ES}$ = 6.07041(4) g, respectively. Here and hereafter, unless otherwise specified, the brackets refer to the standard uncertainty. The residuals of the fitted data were on average within ± 0.02 mg. However, since there are also spikes up to 0.04 mg, an uncertainty of 0.04 mg was assigned to the measured masses.

### *Preparation of the irradiation samples*

Two sub-samples, 2 mL volumes, of the measurement solution, hereafter called samples, were taken and pipetted in two different 8 mL polyethylene (PE) vials. Afterwards, 80 filter paper disks (12 mm diameter) obtained from a single sheet using a cutting punch were inserted in both the PE vials. The paper disks were subsequently dried using an IR lamp and pressed using a slice of a 3 mL vial sealed to the 8 mL vial. It was assumed that the Mo and Co content of the pipetted solutions precipitates completely in the paper disks; this was confirmed by subsequent measurements with the emptied PE vials. The preparation of a sample for irradiation is summarized in Fig. 1.

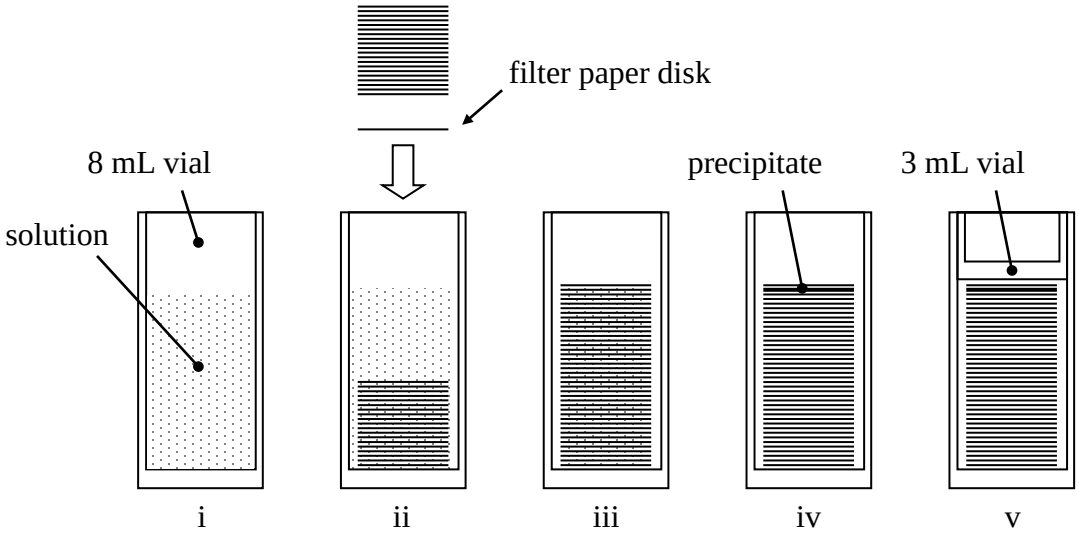


**Fig. 1** Preparation of an irradiation sample; (i) the pipetted sub-sample of the measurement solution, (ii) and (iii) insertion of the filter paper disks, (iv) paper disks after drying, (v) sealed PE vial

The visual inspection of the PE vials after drying was evidence for a precipitation largely occurring in the upper part of the piled disks (see the picture in Fig. S1). This was proof that the Mo and Co solutes were not homogeneously distributed in the paper disks. Since the mass fraction of the Co solution in the measurement solution was at $10^{-3}$ level, the pipetted 2 mL solution consisted of 2 mg of Mo and the observed precipitate could have been ammonium molybdate tetrahydrate.

To limit the effect of external contaminations, the PE vials, the tweezers used to handle the filter paper disks were cleaned in an ultrasonic bath with diluted $HNO_3$ and the cutting punch was washed with isopropyl alcohol. The water was purified using a

Millipore system ($\rho \geq 18$ MΩ). Concerning the filter paper, a previous neutron activation experiment carried out with the disks did not show any contamination of Co and Mo.

## *Neutron irradiation and gamma spectrometry*

The neutron irradiation lasted 3 h and was performed in the central channel of the 250 kW TRIGA Mark II reactor at the Laboratory of Applied Nuclear Energy (LENA) of the University of Pavia. The nominal thermal and epithermal neutron fluxes were about $6 \times 10^{12}$ cm$^{-2}$ s$^{-1}$ and $5.5 \times 10^{11}$ cm$^{-2}$ s$^{-1}$, resulting in a nominal $f$ value of 10.9. The samples were put in a PE container used for irradiation. Fig. 2 shows the position of the container and the samples with respect to the equator of the reactor core.

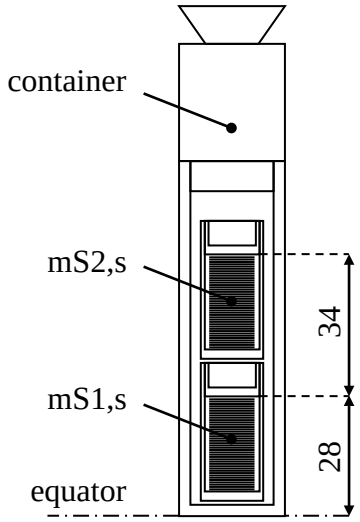


**Fig. 2** Position of the irradiation container and the samples with respect to the equator of the reactor core; dimensions are in mm

After the neutron irradiation, the samples were extracted from the container, rinsed with diluted $HNO_3$ and fixed to a $\gamma$-counting container (Fig. 3).

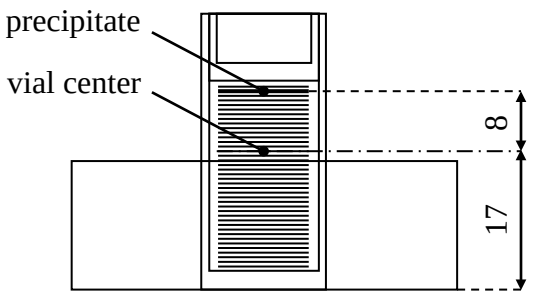


**Fig. 3** Position of the sample with respect to the $\gamma$-counting containers; dimensions are in mm

The $\gamma$-detection was carried out using a detector Canberra GC3518 (relative efficiency 35 %, 1.80 keV FWHM resolution at 1332 keV), and a detector ORTEC® GEM50P4-83 (66 mm crystal diameter, 50 % relative efficiency, 1.90 keV FWHM resolution at 1332 keV).

Six $\gamma$-spectrometry sequences were recorded with a digital signal processor ORTEC® DSPEC 502 and a personal computer running the software for data acquisition ORTEC® Gamma Vision [6]. The first four sequences were performed with the GC3518 and concerned the 140.51 keV $\gamma$-emission of $^{99}$Mo and $^{99m}$Tc in equilibrium conditions. The latter two $\gamma$-spectrometry sequences were performed with the GEM50P4-83 and concerned the 1173.23 keV and 1332.49 keV $\gamma$-emission of $^{60}$Co. Each sequence consisted of $n$ counts performed by adjusting on-line the counting window to reach a 0.23 % counting uncertainty. The dead to counting time ratio, $t_{dead} / t_c$, of the detection systems during the data collection was always below 2.5 %. The position of the $\gamma$-counting containers with respect to the detector during the first four and the latter two sequences are displayed in Fig. 4a and Fig. 4b, respectively. In particular, the distances between the bottom of the $\gamma$-counting container and the end-cap of the detector were $d_{GC3518}$ = 230 mm and $d_{GEM50P4-83}$ = 85 mm.

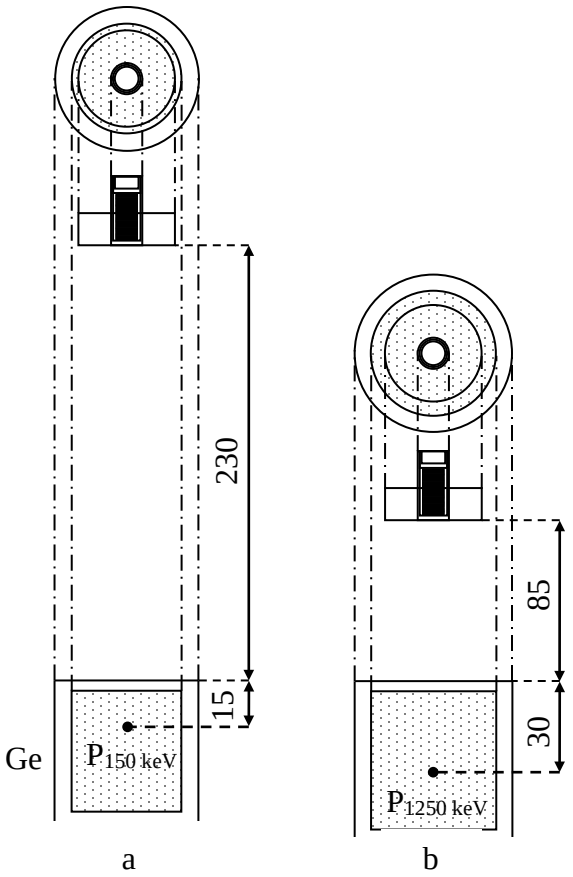


**Fig. 4** Position of the $\gamma$-counting containers (a) with respect to the detector GC3518 during $^{99}$Mo and $^{99m}$Tc detection and (b) with respect to the detector GEM50P4-83 during the $^{60}$Co detection. The point $P_{E\gamma}$ defines the (virtual) vertical position within the Ge crystal where the detection efficiency $\varepsilon$ tends to infinite; dimensions are in mm

The sequence number, the sample, the decay time at the beginning of the sequence, $t_{d\,1}$, and the number of collected counts, $n$, are summarized in table 1. The first sequence started about 4 days after the end of the irradiation to assure a negligible effect due to the $^{99}$Mo and $^{99m}$Tc equilibrium conditions [5].

**Table 1** The sample, the decay time, $t_{d\,1}$, and the number of collected counts, $n$, in each sequence

| sequence | sample | $t_{d\,1}$ / h | counts / $n$ |
|---|---|---|---|
| 1 | mS1,s | 94.1 | 17 |
| 2 | mS2,s | 118.3 | 38 |
| 3 | mS1,s | 152.9 | 36 |
| 4 | mS2,s | 163.6 | 27 |

| | | | |
|---|---|---|---|
| 5 | mS1,s | 692 | 14 |
| 6 | mS2,s | 1058 | 22 |

## Results and discussion

The count rate of the $i^{th}$ count of the sequence, $C_i(t_d)$, was computed according to (8). The decay constants, $\lambda = \ln(2) / t_{1/2}$, were calculated using the half-life literature values, i.e. $t_{1/2}(^{99}\text{Mo}, ^{99m}\text{Tc}) = 65.976(24)$ h (in equilibrium conditions) and $t_{1/2}(^{60}\text{Co}) = 1925.28(14)$ d [7, 8]. The net count, $n_{c\,i}$, was obtained by fitting the full-energy $\gamma$-peak with the algorithm implemented on the Gamma Vision software (analysis engine wan32 G53W2.06).

The 140.51 keV $^{99}$Mo, $^{99m}$Tc count rates, extrapolated to $t_{d\,mS1,s} = 94.1$ h and $t_{d\,mS2,s} = 118.3$ h, are reported in Fig. 5. Here and hereafter, the error bars indicate the 95 % confidence interval due to counting statistics.

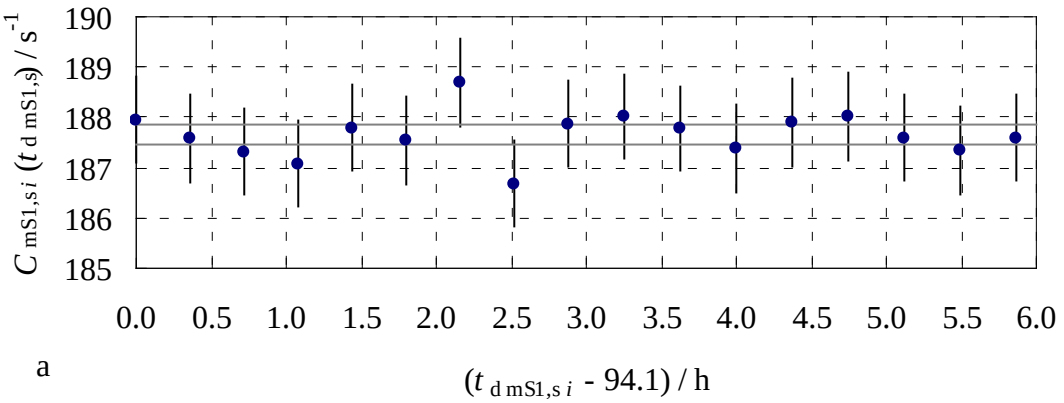


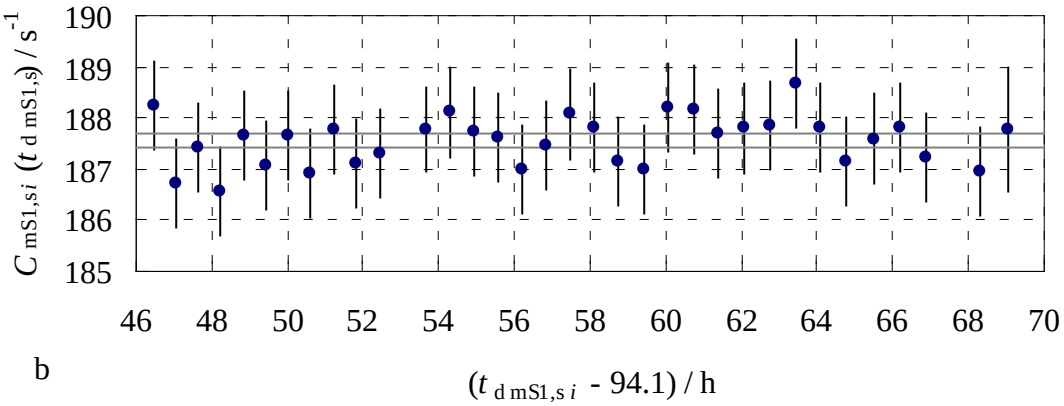

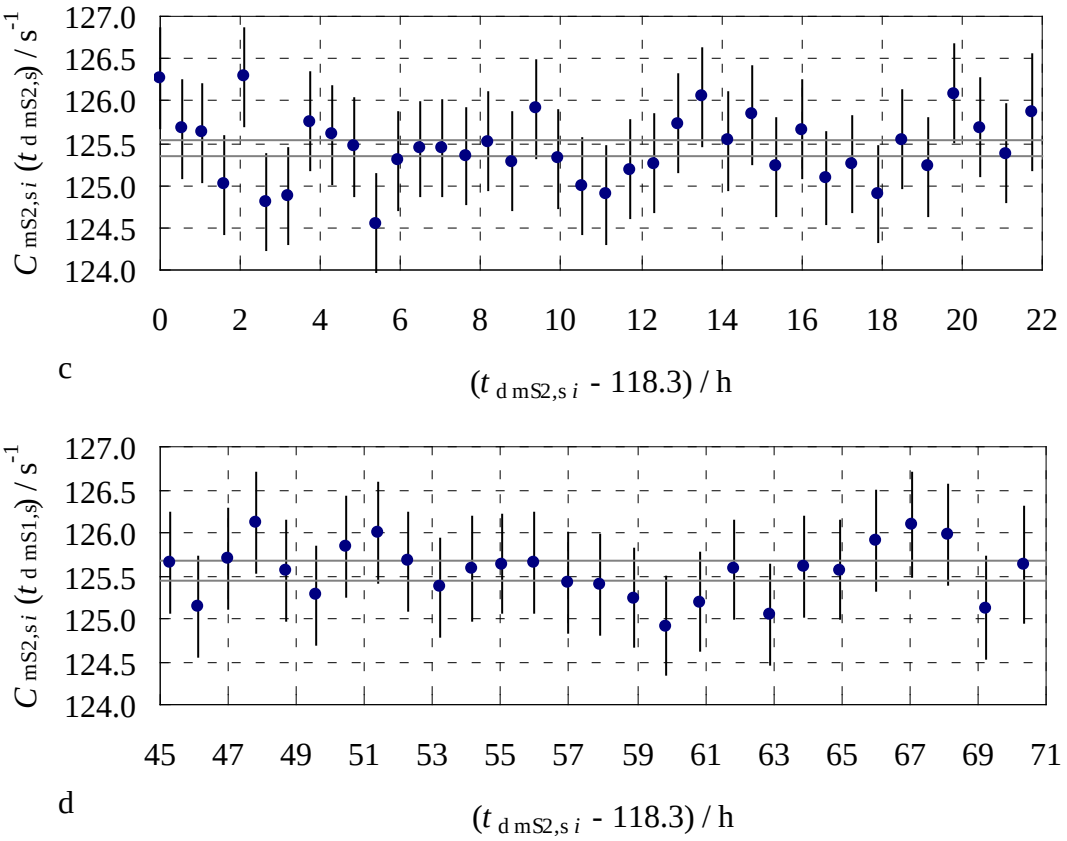


**Fig. 5** The 140.51 keV $^{99}$Mo, $^{99m}$Tc count rates of the mS1,s sample extrapolated to $t_{\mathrm{d\,mS1,s}}$ = 94.1 h and recorded during (a) the sequence 1 and (b) the sequence 3. The 140.51 keV $^{99}$Mo, $^{99m}$Tc count rates of the mS2,s sample extrapolated to $t_{\mathrm{d\,mS2,s}}$ = 118.3 h and recorded during (c) the sequence 2 and (d) the sequence 4. The horizontal lines show the 95 % confidence interval associated to the mean of the count rate values

The mean values of the 140.51 keV $^{99}$Mo, $^{99m}$Tc count rates recorded with the mS1,s and the mS2,s samples, extrapolated to $t_{\mathrm{d\,mS1,s}}$ = 94.1 h and $t_{\mathrm{d\,mS2,s}}$ = 118.3 h, were $C_{\mathrm{mS1,s}}(t_{\mathrm{d\,mS1,s}})$ = 187.589(61) s$^{-1}$ and $C_{\mathrm{mS2,s}}(t_{\mathrm{d\,mS2,s}})$ = 125.486(36) s$^{-1}$, respectively (uncertainties are due to counting statistics). The horizontal lines in Fig. 5 show the 95 % confidence interval associated to the mean of the count rates values. The count rate ratio, $\frac{C_{\mathrm{mS1,s}}(t_{\mathrm{d\,mS1,s}})}{C_{\mathrm{mS2,s}}(t_{\mathrm{d\,mS2,s}})}$, was 1.49490(65) s$^{-1}$.

The 1173.23 keV and 1332.49 keV $^{60}$Co count rates are reported in Fig. 6.

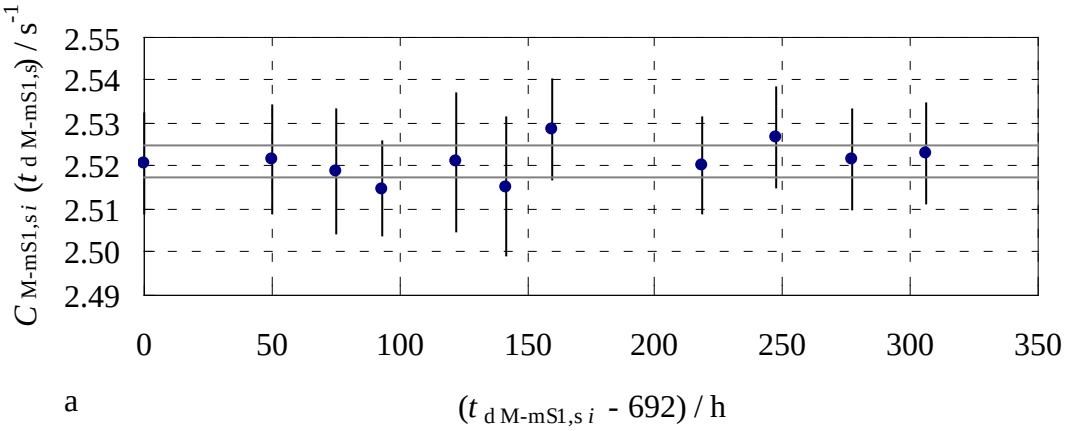
$C_{\mathrm{M\text{-}mS1},s\,i}\,(t_{\mathrm{d\,M\text{-}mS1},s\,i})\,/\,\mathrm{s}^{-1}$
2.55
2.54
2.53
2.52
2.51
2.50
2.49
0
50
100
150
200
250
300
350
$(t_{\mathrm{d\,M\text{-}mS1},s\,i}\,-\,692)\,/\,\mathrm{h}$

a

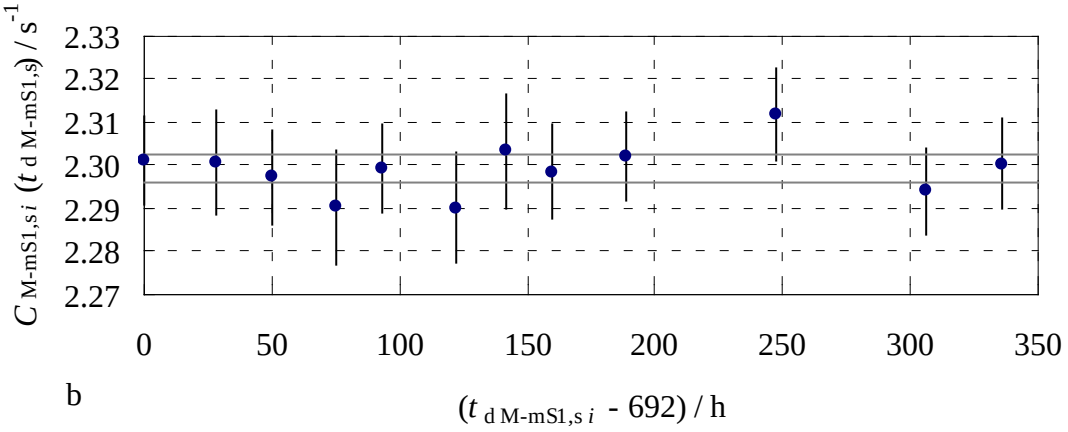
$C_{\mathrm{M\text{-}mS1},s\,i}\,(t_{\mathrm{d\,M\text{-}mS1},s\,i})\,/\,\mathrm{s}^{-1}$
2.33
2.32
2.31
2.30
2.29
2.28
2.27
0
50
100
150
200
250
300
350
$(t_{\mathrm{d\,M\text{-}mS1},s\,i}\,-\,692)\,/\,\mathrm{h}$

b

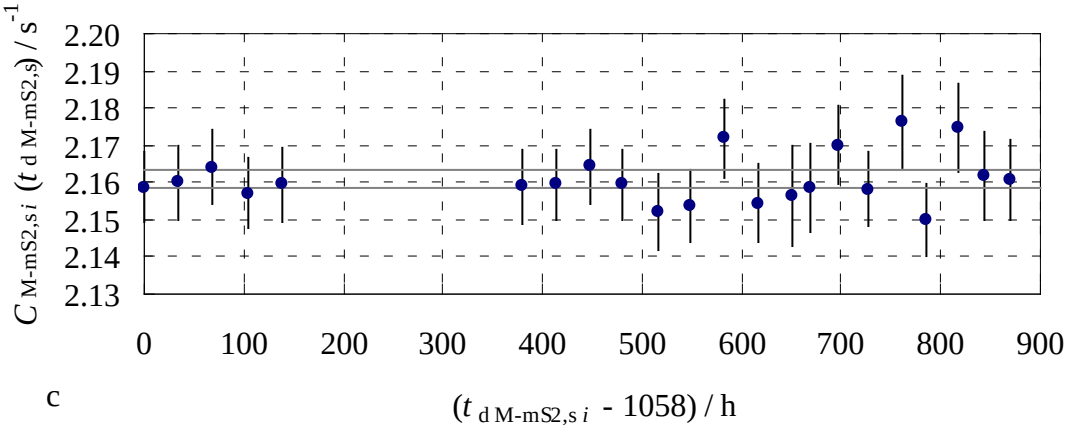
$C_{\mathrm{M\text{-}mS2},s\,i}\,(t_{\mathrm{d\,M\text{-}mS2},s\,i})\,/\,\mathrm{s}^{-1}$
2.20
2.19
2.18
2.17
2.16
2.15
2.14
2.13
0
100
200
300
400
500
600
700
800
900
$(t_{\mathrm{d\,M\text{-}mS2},s\,i}\,-\,1058)\,/\,\mathrm{h}$

c

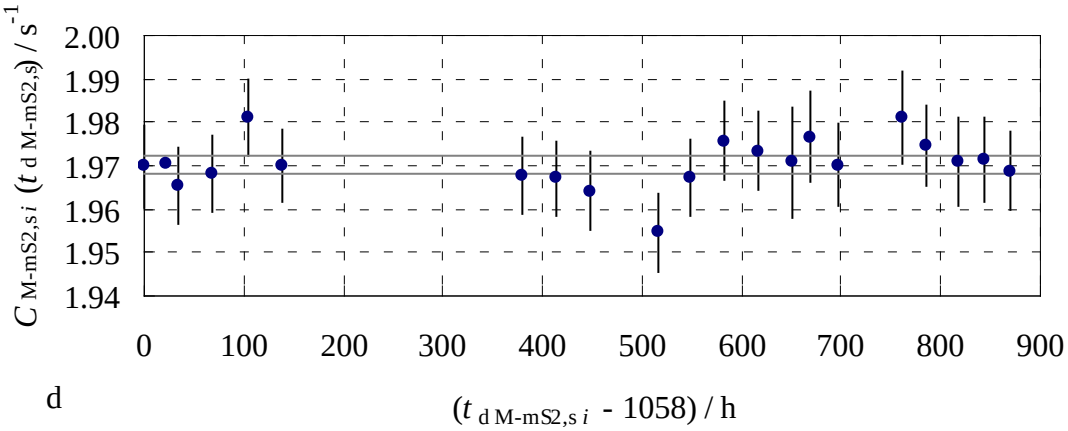


**Fig. 6** (a) The 1173.23 keV and (b) the 1332.49 keV $^{60}$Co count rates of the mS1,s sample recorded during the sequence 5 and extrapolated to $t_{\mathrm{d\ M\text{-}mS1,s}} = 692$ h. (c) The 1173.23 keV and (d) the 1332.49 keV $^{60}$Co count rates of the mS2,s sample recorded during the sequence 6 and extrapolated to $t_{\mathrm{d\ M\text{-}mS2,s}} = 1058$ h. The horizontal lines show the 95 % confidence interval associated to the mean of the count rate values

The mean values of the 1173.23 keV $^{60}$Co count rates recorded with the mS1,s and the mS2,s samples, extrapolated to $t_{\mathrm{d\ M\text{-}mS1,s}} = 692$ h and $t_{\mathrm{d\ M\text{-}mS2,s}} = 1058$ h, were $C_{\mathrm{M\text{-}mS1,s}}(t_{\mathrm{d\ M\text{-}mS1,s}}) = 2.5212(19)\ \mathrm{s^{-1}}$ and $C_{\mathrm{M\text{-}mS2,s}}(t_{\mathrm{d\ M\text{-}mS2,s}}) = 2.1609(11)\ \mathrm{s^{-1}}$, respectively; the mean values of the 1332.49 keV $^{60}$Co count rates recorded with the mS1,s and the mS2,s samples, extrapolated to $t_{\mathrm{d\ M\text{-}mS1,s}} = 692$ h and $t_{\mathrm{d\ M\text{-}mS2,s}} = 1058$ h, were $C_{\mathrm{M\text{-}mS1,s}}(t_{\mathrm{d\ M\text{-}mS1,s}}) = 2.2991(16)\ \mathrm{s^{-1}}$ and $C_{\mathrm{M\text{-}mS2,s}}(t_{\mathrm{d\ M\text{-}mS2,s}}) = 1.9704(10)\ \mathrm{s^{-1}}$, respectively (uncertainties are due to counting statistics). The horizontal lines in Fig. 6 show the 95 % confidence interval associated to the mean of the $^{60}$Co count rates values. The weighted mean value of the count rate ratios, $\left.\dfrac{C_{\mathrm{M\text{-}mS2,s}}(t_{\mathrm{d\ M\text{-}mS2,s}})}{C_{\mathrm{M\text{-}mS1,s}}(t_{\mathrm{d\ M\text{-}mS1,s}})}\right|_{\mathrm{m}}$, was 0.85708(55) $\mathrm{s^{-1}}$.

## *Correction Factors*

The differences $t_{\mathrm{d\ mS2,s}} - t_{\mathrm{d\ mS1,s}}$ and $t_{\mathrm{d\ M\text{-}mS2,s}} - t_{\mathrm{d\ M\text{-}mS1,s}}$ were 24.2 h and 366 h, respectively, i.e. about 0.4 times $t_{1/2}(^{99}\mathrm{Mo}, ^{99\mathrm{m}}\mathrm{Tc})$ and $8 \times 10^{-3}$ times $t_{1/2}(^{60}\mathrm{Co})$. Accordingly, $\kappa_{\mathrm{td}} = 0.77554$ and $\kappa_{\mathrm{M\text{-}td}} = 0.99452$ with negligible uncertainties.

The measurement solutions had a similar Mo and Co mass fraction and the pipetted subsamples had the same volume. In the case of a 1 mm thick, 12 mm diameter sample with 2 mg Mo and 10 μg Co, the neutron self-shielding factor is 0.998 for Mo and 1.000 for Co, i.e. 0.2 % epithermal neutron self-shielding for Mo. Even if the solutes were not uniformly distributed in the paper disks, the neutron self-shielding factors $k_{\text{ss mS1,s}} = k_{\text{ss mS2,s}}$, $k_{\text{M-ss mS1,s}} = k_{\text{M-ss mS2,s}}$. Similarly, the $\gamma$-self-absorption factors $k_{\text{sa mS1,s}} = k_{\text{sa mS2,s}}$, $k_{\text{M-sa mS1,s}} = k_{\text{M-sa mS2,s}}$ and the geometry factors $k_{\text{g mS1,s}} = k_{\text{g mS2,s}}$, $k_{\text{M-g mS1,s}} = k_{\text{M-g mS2,s}}$. Thus, $\kappa_{\text{ss}} = \kappa^{-1}_{\text{M-ss}} = \kappa_{\text{sa}} = \kappa^{-1}_{\text{M-sa}} = \kappa_{\text{g}} = \kappa^{-1}_{\text{M-g}} = 1$ with negligible uncertainty.

The full-energy $\gamma$-peak detection efficiency $\varepsilon$ tends to infinite in a (virtual) vertical position within the Ge crystal of the detector [9]. This position depends on the $\gamma$-photon energy, $E_\gamma$, and is defined by a point, $\text{P}_{\text{E}\gamma}$ (see Fig. 4). A previous characterization of the detectors showed that the distance between the end-cap and $\text{P}_{\text{E}\gamma}$ is $d_{150\text{ keV}} = 15$ mm for the GC3518 and $d_{1250\text{ keV}} = 30$ mm for the GEM50P4-83. The distance betwen the center of the PE vial and the bottom of the $\gamma$-counting container, $d_{\text{c}}$, and the distance between the center of the PE vial and the precipitate, $d_{\text{p}}$, were 17 mm and 8 mm, respectively (see Fig. 3). The detection efficiency correction factors are

$$\kappa_{\varepsilon} = \frac{(d_{\text{Mo}} + \Delta d_{\text{Mo2}})^2}{(d_{\text{Mo}} + \Delta d_{\text{Mo1}})^2} \text{ and } \kappa_{\text{M-}\varepsilon} = \frac{(d_{\text{Co}} + \Delta d_{\text{Co2}})^2}{(d_{\text{Co}} + \Delta d_{\text{Co1}})^2}, \tag{16}$$

where $\Delta d_{\text{Mo1}}$ and $\Delta d_{\text{Mo2}}$ are the distances between the Mo center of mass and the center of the PE vial in sample 1 and 2, $\Delta d_{\text{Co1}}$ and $\Delta d_{\text{Co2}}$ are the distances between the Co center of mass and the center of the PE vial in sample 1 and 2, $d_{\text{Mo}} = d_{\text{150keV}} + d_{\text{GC3518}} + d_{\text{c}} = 262$ mm and $d_{\text{Co}} = d_{\text{1250keV}} + d_{\text{GEM50P4-83}} + d_{\text{c}} = 132$ mm. As examples, if in both the samples all the Mo and Co were in the precipitate, i.e. $\Delta d_{\text{Mo1}} = \Delta d_{\text{Mo2}} = \Delta d_{\text{Co1}} = \Delta d_{\text{Co2}} = d_{\text{p}}$, $\kappa_{\varepsilon} = \kappa^{-1}_{\text{M-}\varepsilon} = 1$. Instead, if in sample 2 only a fraction of Mo and Co was in the precipitate, i.e. $\Delta d_{\text{Mo1}} = \Delta d_{\text{Co1}} = d_{\text{p}}$ and $\Delta d_{\text{Mo2}} = \Delta d_{\text{Co2}} = d_{\text{p}} - \Delta d_{\text{p}}$, in the case of $\Delta d_{\text{p}} = 4$ mm, $\kappa_{\varepsilon} = 0.985$ and $\kappa_{\text{M-}\varepsilon} = 0.971$.

Since the actual positions of Mo and Co centers of mass were not measured, $\Delta d_p = \pm 4$ mm (uniform distribution) was preliminary assigned. Accordingly, $\kappa_{\varepsilon} = 1.000(9)$ and $\kappa_{M\text{-}\varepsilon} = 1.000(16)$.

The literature $Q_0$ values for $^{98}$Mo and $^{59}$Co are 53.1(33) and 1.993(60) [10]. Experimental data for the $\alpha$ value at the LENA irradiation channel are missing. However, based on the $\alpha$ = -0.051(8) value at the central channel of the TRIGA Mark II reactor operating in Ljubljana [11], from (9) it follows that $Q_{0,Mo}(\alpha) = 70(9)$, $Q_{0,Co}(-0.051) = 2.5(6)$ and $\alpha_Q = -0.965(10)$.

Due to the 10.9 nominal $f$ value, about 85% of the $^{60}$Co activity was produced by thermal neutrons. As the $^{60}$Co count rate of sample 2 to the count rate of sample 1 ratio was about 0.86, the $\Phi_{th1}$ was approximately 16 % higher than $\Phi_{th2}$ and a possible variation of $f$ could be expected. In the case of $\alpha_f = \pm 0.025$ (uniform distribution) and 10 % relative uncertainty for the $f$ value, $\beta_R = 1.000(10)$.

## *Uncertainty budget*

The application of (15) to the experimental data collected in this study gave a ratio $\tau = 0.999(19)$. The provisional uncertainty budget calculated according to the Guide to the Expression of Uncertainty in Measurement [12] is reported in table 2.

**Table 2** Uncertainty budget of the measured ratio $\tau$. The input quantities $x_i$ are given in the text. The index column gives the relative contributions of $u(x_i)$ to the combined standard uncertainty, $u_c(y)$, of $\tau$

| Quantity | Unit | Value | Standard uncertainty | Index |
|---|---|---|---|---|
| $X_i$ | $[X_i]$ | $x_i$ | $u(x_i)$ | % |
| $m_{1,MS}$ | g | 0.12572 | 0.00004 | 0.0 |
| $m_{2,MS}$ | g | 0.12572 | 0.00004 | 0.0 |
| $m_{ES1}$ | g | 27.03259 | 0.00006 | 0.0 |

| | | | | |
|---|---|---|---|---|
| $m_{ES2}$ | g | 27.03259 | 0.00006 | 0.0 |
| $C_{mS1,s}/C_{mS2,s}$ | 1 | 1.49490 | 0.00065 | 0.0 |
| $C_{M\text{-}mS2,s}/C_{M\text{-}mS1,s}$ | 1 | 0.85708 | 0.00055 | 0.1 |
| $\beta_R$ | 1 | 1.000 | 0.010 | 22.8 |
| $\kappa_{td}$ | 1 | 0.77554 | 0.00000 | 0.0 |
| $\kappa_{M\text{-}td}$ | 1 | 0.99452 | 0.00000 | 0.0 |
| $\kappa_{ss}$ $(\kappa_{M\text{-}ss})^{-1}$ | 1 | 1.00000 | 0.00000 | 0.0 |
| $\kappa_{sa}$ $(\kappa_{M\text{-}sa})^{-1}$ | 1 | 1.00000 | 0.00000 | 0.0 |
| $\kappa_{g}$ $(\kappa_{M\text{-}g})^{-1}$ | 1 | 1.00000 | 0.00000 | 0.0 |
| $\kappa_{\varepsilon}$ | 1 | 1.000 | 0.009 | 18.5 |
| $\kappa_{M\text{-}\varepsilon}$ | 1 | 1.000 | 0.016 | 58.5 |
| $Y$ | $[Y]$ | $y$ | $u_c(y)$ | |
| $\tau$ | 1 | 0.999 | 0.019 | 100.0 |

Given that the variation of the shape of the neutron energy spectrum and the detection efficiency were the main influence factors, the following ways are suggested to reduce their effects.

In particular, the measurement model shows that the adoption of a monitor element having a $Q_0$ value similar to the $Q_0$ value of $^{99}$Mo makes the result almost independent on $f$, $\alpha$, $Q_{0,E}$, and $Q_{0,EM}$ values. The best choice among the potential target elements is the $^{116}$Sn, which is neutron activated to $^{117}$Sn via (n,γ) capture reaction and detected via the 158.56 keV $\gamma$-photons emitted during the radioactive decay of $^{117}$Sn ($t_{1/2}$ = 13.76(4) d [13]). The outcome of the $Q_0$ = 56.3(11) value [10] of $^{116}$Sn might be a $\beta_R$ = 1 with a relative uncertainty below 0.01 %.

Moreover, the actual position of the radionuclide center of mass with respect to the center of the 8 mL PE vial can be experimentally determined by counting the sample right-side-up and up-side-down. See equation (S1) in the supplementary information for detail. Hence, the knowledge of the $\Delta d_p$ value and the increase of the distance of the samples

from the detector during the $\gamma$-counting might limit the $\kappa_{\varepsilon}$ and $\kappa_{M\text{-}\varepsilon}$ relative uncertainty below 0.1 %.

## Conclusions

The possibility of using the INAA technique to determine the ratio of the mass fractions of two mono-elemental solutions with a relative expanded uncertainty of less than 0.1 % was investigated. To reach the target uncertainty, the addition of a monitor solution to the elemental solution was essential to correct for possible variation of the neutron energy spectrum at the irradiation positions. A procedure was developed and the related measurement model was obtained from the neutron activation equation.

The proposed measurement procedure was applied in a feasibility test in the case of two Mo solutions having the same mass fraction, i.e. obtained from the same solution, and using Co as the monitor element. The departure of the measured ratio from the unit value (-0.1 %) was in agreement with the evaluated 1.9 % relative uncertainty. The uncertainty budget pointed out that the main contributors were the variation of the shape of the neutron energy spectrum and the detection efficiency.

The target 0.1 % relative expanded uncertainty was not achieved. Nevertheless, the use of INAA to link up Mo solutions to the SI is promising; a considerable decrease of the measurement uncertainty might be reached by improved sample preparation and an improved $\gamma$-counting technique.

## Acknowledgements

Financial support by the European Metrology Research Programme (EMRP) is gratefully acknowledged (EMRP-SIB09 “Purity standards for challenging elements”) [14]. The EMRP is jointly funded by the EMRP participating countries within the European Association of National Metrology Institutes (EURAMET). The authors are grateful to the referee for providing constructive comments and help in improving the contents of this paper.

## References

1. D'Agostino G, Bergamaschi L, Giordani L, Oddone M, Kipphardt H, Richter S (2014) Use of Instrumental Neutron Activation Analysis to investigate the distribution of trace elements among subsamples of solid materials. Metrologia 51:48-53
2. Kaltenbach A, Noordmann J, Görlitz V, Pape C, Richter S, Kipphardt H, Kopp G, Jährling R, Rienitz O, Güttler B (2015) Gravimetric preparation and characterization of primary reference solutions of molybdenum and rhodium. Anal Bioanal Chem 407:3093-3102
3. Rienitz O, Schiel D, Görlitz V, Jährling R, Vogl J, Lara-Manzano J V, Zoń A, Fung W H, Buzoianu M, Caciano de Sena R, Augusto dos Reis L, Valiente L, Yim Y H, Hill S, Champion R, Fisicaro P, Bing W, Turk G C, Winchester M R, Saxby D, Merrick J, Hioki A, Miura T, Suzuki T, Linsky M, Barzev A, Máriássy M, Cankur O, Ari B, Tunç M, Konopelko L A, Kustikov Y A, Bezruchko M (2012) Final report on CCQM-K87: Mono-elemental calibration solutions. Metrologia DOI 10.1088/0026-1394/49/1A/08010
4. Høgdahl OT (1965) Proceedings of the Symposium on Radiochemical Methods of Analysis 1:23-40
5. De Corte F (1987) The k0-Standardisation Method. A move to the optimization of Neutron Activation Analysis. Ed. Ryksuniversiteit Gent Faculteit Van de Wettenschappen
6. GammaVision (2006) Version 6.08; Advanced Measurement Technology, Inc.: Berwyn, PA
7. Browne E, Tuli J K (2011) Nucl Data Sheets 112:275-446
8. Browne E, Tuli J K (2013) Nucl Data Sheets 114:1849-2022
9. Gilmore G, Hemingway J D (1995) Practical Gamma-ray Spectrometry, New York, Wiley
10. Kolotov VP, De Corte F (2004) Compilation of $k_0$ and related data for NAA in the form of electronic database (IUPAC Technical Report). Pure Appl. Chem. 76:1921-1925

11. Jovanovic S, Vukotic P, Smodis B, Jacimovic R, Mihaljevic N, Stegnar P (1989) Epithermal neutron flux characterization of the TRIGA Mark II reactor, Ljubljana, Yugoslavia, for use in NAA. J. Radioanal. Nucl. Chem. 129:343-349
12. JGCM 100:2008 (2008) Evaluation of measurement data - Guide to the expression of uncertainty in measurement
13. Blachot J (2002) Nucl Data Sheets 95:679-836
14. Online available at http://www.ptb.de/emrp/sib09.html

# Supplementary information

## *Irradiation samples*

**Fig. S1** The precipitates in the upper part of the piled disks of the PE vials after drying

## *Position of the radionuclide center of mass*

The distance between the radionuclide center of mass with respect to the center of the 8 mL PE vial, $\Delta d$, can be determined by using the following formula:

444
$$\frac{C_{\mathrm{rsu}}(t_{\mathrm{d}})}{C_{\mathrm{usd}}(t_{\mathrm{d}})} = \frac{1 - \frac{\Delta d}{d}}{1 + \frac{\Delta d}{d}}, \qquad \text{(S1)}$$

445 where $C_{\mathrm{rsu}}(t_{\mathrm{d}})$, $C_{\mathrm{rsd}}(t_{\mathrm{d}})$ are the count rates recorded with the right-side-up and up-side-
446 down sample, respectively, and $d$ is the distance between the center of the 8 mL PE vial
447 and the (virtual) vertical position where the detector efficiency tends to infinite.